Detecting local ligand-binding site similarity in nonhomologous proteins by surface patch comparison

Lee Sael[1,2,3] and Daisuke Kihara[1,2,3]*

[1] Department of Computer Science, Purdue University, West Lafayette, Indiana 47907

[2] Department of Biological Sciences, Purdue University, West Lafayette, Indiana 47907

[3] Markey Center for Structural Biology, Purdue University, West Lafayette, Indiana 47907

ABSTRACT

Functional elucidation of proteins is one of the essential tasks in biology. Function of a protein, specifically, small ligand molecules that bind to a protein, can be predicted by finding similar local surface regions in binding sites of known proteins. Here, we developed an alignment free local surface comparison method for predicting a ligand molecule which binds to a query protein. The algorithm, named Patch-Surfer, represents a binding pocket as a combination of segmented surface patches, each of which is characterized by its geometrical shape, the electrostatic potential, the hydrophobicity, and the concaveness. Representing a pocket by a set of patches is effective to absorb difference of global pocket shape while capturing local similarity of pockets. The shape and the physicochemical properties of surface patches are represented using the 3D Zernike descriptor, which is a series expansion of mathematical 3D function. Two pockets are compared using a modified weighted bipartite matching algorithm, which matches similar patches from the two pockets. Patch-Surfer was benchmarked on three datasets, which consist in total of 390 proteins that bind to one of 21 ligands. Patch-Surfer showed superior performance to existing methods including a global pocket comparison method, Pocket-Surfer, which we have previously introduced. Particularly, as intended, the accuracy showed large improvement for flexible ligand molecules, which bind to pockets in different conformations.

Key words: structure-based function prediction; protein surface shape; ligand-binding pocket; 3D Zernike descriptors; pocket comparison.

INTRODUCTION

Elucidating function of uncharacterized proteins is one of the most important tasks in molecular biology. Bioinformatics is expected to play a significant role for this task given the fact that computational methods are quick in screening existing data.[1–5] Function annotation for newly determined genes and genomes by sequence database searches[6] has long become a routine in wet biology laboratories. Recently, the urgent need was raised for function elucidation for protein structures due to the increasing number of protein structures of unknown function that have been solved by structural genomics projects.[7] As of this writing, there are over 3200 structures of unknown function deposited in the Protein Data Bank (PDB).[8] In the post structural genomics era, making use of protein structure data for functional studies both by high-throughput experimental methods and computational methods is of the highest priority.[9–11]

Function of proteins has broad meaning and can be classified into different semantic classes. For example, the Gene Ontology[12] classifies vocabulary of functional terms into three major categories, biological process, molecular function, and cellular component. In this work, we focus on predicting binding small ligand molecules for proteins. Ligand binding is an essential role of proteins in a cell and thus provides clues of protein function in all the GO categories. Binding ligand prediction also has a broader impact to applications such as computational drug discovery[13] and protein design.[14]

A binding ligand for an uncharacterized protein can be predicted by evaluating the similarity of either the whole protein structure[15] or the binding pocket to those of known proteins in the database. Pocket comparison methods have an advantage over global structure comparison-based methods because the former could detect similar pockets independent from homologous relationship of proteins. Indeed, there are numerous examples of proteins that are evolutionary unrelated yet bind the same ligand molecule.[16] There are several approaches proposed for

pocket comparison in the past. In the Catalytic Site Atlas,[17] AFT,[18] and SURFACE,[19] a functional site is represented as a set of few residue positions and the root mean square deviation (RMSD) is computed as the measure of the similarity between a query and a site in the database. SiteBase[20] and MultiBind[21] use geometric hashing for comparing conformation of pseudocenters of residues in ligand-binding sites. A method introduced by Hoffmann et al.[22] applies a convolution kernel method for comparing surface atom positions and charges at ligand-binding sites.

An alternative approach to the residue/atom-based representations is to describe protein surface of a binding pocket.[23] A surface representation describes geometrical and physicochemical properties of a pocket on a continuous surface often discarding residue type information. Thus, they are less dependent on available homologous structures from which the features are extracted. The eF-seek method represents a protein surface as a graph with nodes charactering local geometry and the electrostatic potential.[24] A maximum subgraph matching algorithm is used for seeking similar sites in two proteins. The Thornton group explored the use of spherical harmonics in representing and comparing protein pockets.[25,26] The property-encoded shape distributions method by Das et al.[27] extended the D2 shape distribution method[28] so that surface properties can also be incorporated. In our previous work, we introduced a pose independent binding pocket comparison method, named Pocket-Surfer, which uses the pseudo-Zernike descriptors and the 3D Zernike descriptors (3DZD) to quantify the similarity of the global surface shape and the electrostatic potential of binding pockets.[29] Pocket-Surfer allows real-time pocket database search, and it was shown that it performed superior to existing methods.[5,29]

These pocket comparison methods describe the property of binding pockets as a whole. However, studies have found that often binding pockets of the same ligand show variation in their shape and physicochemical properties.[26,30] The variation in the geometrical and physicochemical properties is due to several different reasons. For example, some ligand molecules can take different conformations on binding. Often, additional ligand molecules or water molecules bind at the same pocket, which results in change in the overall pocket shape and associated properties. However, even with such pockets that do not exhibit overall shape and physicochemical similarity, there are usually local regions that show consistent properties across different proteins. Based on this observation, we propose a new perspective on binding site comparisons, which evaluates the similarity of binding pockets by the combination of similarity of its local patch regions. The proposed method, named Patch-Surfer, segments the binding pockets to circular patches and compares them using a weighted bipartite matching algorithm. Two geometric properties, the surface shape and the visibility,[31] and two physicochemical prosperities, the hydrophobicity and the electrostatic potential, of the patches are encoded with the

3DZD, a mathematical series expansion of a three-dimensional function,[32] which offers a compact and rotationally invariant representation of the patch properties.

We benchmarked Patch-Surfer on three binding pocket datasets. Pocket retrieval results on the first dataset compiled by Kahraman et al.[33] showed that Patch-Surfer performed overall better than Pocket-Surfer,[29] our previously developed pocket comparison method that captures global similarity of pockets. Then the parameters trained on the Kahraman dataset were further tested on the extended Kahraman dataset to examine the transferability of the parameters. Subsequently, the result of the third dataset, the Huang[34] dataset, was shown to validate that Patch-Surfer can perform well for different sets of ligand-binding pockets. The method was further applied for ligand unbound and predicted pockets. Overall, Patch-Surfer showed better accuracy compared with Pocket-Surfer[29] and other pocket descriptors. As intended, the accuracy showed large improvement for flexible ligand molecules, which bind to pockets in different conformations. Further, Patch-Surfer allows a fast ligand pocket database screening owing to the compact representation of patches with the 3DZD. A search against a database of over 5000 representative pockets (the current size of PDB) takes approximately only 3 min 20 s.

MATERIALS AND METHODS

Ligand-binding pocket datasets

Three datasets of ligand-binding pockets were used for benchmark. The datasets consist of the tertiary protein structures with a bound ligand molecule, which are solved by X-ray crystallography. Redundancy of entries was removed so that sequence similarity between any pairs of proteins in each dataset is kept under 30%. The first dataset, compiled by Kahraman et al.[33] consists of 100 pockets, each of which binds to one of the following nine ligands: adenosine monophosphate (AMP), adenosine-5′-triphosphate (ATP), flavin adenine dinucleotide (FAD), flavin mononucleotide (FMN), alpha- or beta-D-glucose (GLC), heme (HEM), nicotinamide adenine dinucleotide (NAD), phosphate (PO4), or 3-beta-hydroxy-5-androsten-17-one (AND), and estradiol (EST), which are two types of steroids (STR). Table IA lists detailed information the binding pockets. This dataset has been also used in our previous work of Pocket-Surfer.[29]

The second dataset, the extended Kahraman dataset (Table IB), is designed to test the transferability of the parameters trained with the original Kahraman dataset. The dataset consists of 144 proteins that bind to one of the following eight ligands, AMP, ATP, FAD, FMN, GLC, HEM, NAD, and PO4, as listed in the Table IB. This dataset provides different structures to the same ligand molecules as the original Kahraman set. STR was removed from this dataset because STR contains two

Table IA
The Ligand Pocket Benchmark Dataset From Kahraman et al.[33]

Binding ligand molecule	Average size[a] (Å)	Molecular mass (g/mol)	Average number of seeds[b]	Number of PDB entries	PDB entries
AMP	8.8	347.22	23.7	9	12asA, 1amuA, 1c0aA, 1ct9A, 1jp4A, 1khtB, 1qb8A, 1tb7B, 8gpbA
ATP	9.5	507.18	29.5	14	1a0iA, 1a49A, 1aylA, 1b8aA, 1dv2A, 1dy3A, 1e2qA, 1e8xA, 1esqA, 1gn8B, 1kvkA, 1o9tA, 1rdqE, 1tidA
FAD	11	785.55	44.1	10	1cqxA, 1e8gB, 1eviB, 1h69A, 1hskA, 1jqiA, 1jr8B, 1k87A, 1poxA, 3grsA
FMN	9.7	456.34	27.7	6	1dnlA, 1f6vA, 1ja1A, 1mvlA, 1p4cA, 1p4mA
GLC	8.5	180.16	15.2	5	1bdgA, 1cq1A, 1k1wA, 1nf5C, 2gbpA
HEM	10.2	616.49	36.9	16	1d0cA, 1d7cA, 1dk0A, 1eqgA, 1ew0A, 1gweA, 1iqcA, 1nazE, 1np4B, 1po5A, 1pp9C, 1qhuA, 1qlaC, 1qpaB, 1soxA, 2cpoA
NAD	10.1	663.43	36.8	15	1ej2B, 1hexA, 1ib0A, 1jq5A, 1mewA, 1mi3A, 1o04A, 1og3A, 1qaxA, 1rlzA, 1s7gB, 1t2dA, 1toxA, 2a5fB, 2npxA
PO4	7.4	94.97	9.7	20	1a6q, 1b8oC, 1brwA, 1cqjB, 1d1qB, 1dakA, 1e9gA, 1ejdC, 1eucA, 1ew2A, 1fbtB, 1gypA, 1h6lA, 1ho5B, 1l5wA, 1l7mA, 1lbyA, 1lyvA, 1qf5A, 1tcoA
STR	9.2	278.8	22.2	5	1e3rB, 1fdsA, 1j99A, 1lhuA, 1qktA

[a]The pocket size is defined as the average distance from the center of the mass of the pocket to the pocket surface.
[b]The average number of seed points in the pockets.

similar but different molecules as mentioned above. Proteins share the sequence identity of less than 30% to each other within this extended Kahraman dataset and also with any proteins in the original Kahraman dataset (Table IA). In these protein structures, more than 30% of the ligand atoms are within 4.5 Å to the protein surface atoms. The structures of the nine ligands in the Kahraman and the extended Kahraman dataset are shown in Figure 1(A).

The third dataset, the Huang[34] dataset, is for examining pocket retrieval performance of Patch-Surfer on different ligand types as well as on ligand unbound pockets. Total of 146 proteins are selected which bind either one of the following 12 ligand molecules (Table IC): adeno-

sine (ADN), biotin (BTN), fructose 6-phosphate (F6P), fucose (FUC), galactose (GAL), guanine (GUN), mannose (MAN), O1-methyl mannose (MMA), 2-phenylimidazole (PIM), palmitic acid (PLM), retinol (RTL), and 2′-deoxyuridine 5-monophosphate (UMP). From the dataset of the same name used in our previous work,[29] we exchanged several PDB entries so that proteins do not share 30% or more sequence identity within the same ligand-binding proteins and also between proteins with different ligand type. When ligand unbound proteins (rightmost column in Table IC) are used as queries, homologous proteins that share 30% or more sequence identity are removed from the dataset. The structures of the 12 ligands are shown in Figure 1(B).

Table IB
Extended Kahraman Dataset

Binding ligand molecule	Average Size (Å)	Average number of seed	Number of PDB entries	PDB entries
AMP	8.8	22.2	5	1NH8A, 1QGXA, 1Y1PA, 1Z84B, 2R85B
ATP	9.5	32	4	1MJHA, 1OBDA, 1WUAA, 2YW2A
FAD	11	43.5	29	1B5QA, 1C0PA, 1EL5A, 1FOXA, 1F20A, 1F8SA, 1FNDA, 1GPEA, 1JU2A, 1KRHA, 1PBEA, 1PN0B, 1Q1RA, 1RYIA, 1TT0C, 1U8VA, 1W1OA, 1W4XA, 1X0PB, 1YOAA, 1ZK7A, 2BA9A, 2J4DA, 2MBRA, 2OLNA, 2QCUA, 2VFRA, 2YR5A, 2YYJA
FMN	9.7	30.8	8	1D3GA, 1JUEA, 1USCA, 1VYRA, 2D37A, 2H8ZA, 2NR4A, 2PIAA
GLC	8.5	11	9	1JG9A, 1PWBC, 1QK2A, 1RMGA, 1UA4A, 1UOZA, 2J73B, 2V8LA, 3BC9A
HEM	10.2	38.8	26	1BU7A, 1EW6A, 1FS7A, 1FT5A, 1GEJA, 1IO7A, 1IRDA, 1IT2A, 1IW0A, 1J00A, 1KR7A, 1SY7A, 1TU9A, 1U55A, 1W4WA, 1YRCA, 256BA, 2BKMA, 2IJ7A, 2J0PA, 2Q9FA, 2RCHA, 2W31A, 2W3FA, 3B6HA, 3CX5D
NAD	10.1	39.9	15	1C1DB, 1DXYA, 1GIQA, 1GY8D, 1KOLA, 1N2SA, 1OBBB, 1ORRA, 1PL8A, 1R66A, 1SG6A, 1U1IA, 2DVMB, 2H7MA, 2VHXE
PO4	7.4	8.43	48	1A9XA, 1AOPA, 1AQZA, 1DXEA, 1EX2A, 1JE0A, 1K27A, 1KV8A, 1LC0A, 1NV0A, 1OWLA, 1P0KA, 1P1JA, 1PIIA, 1Q11A, 1RKDA, 1RWHA, 1T46A, 1TG7A, 1THFD, 1TZYE, 1V2XA, 1WCHA, 1WOQA, 1XA1B, 1XW3A, 1Y6VA, 1YB0A, 1YN9A, 1YRRA, 1YSQA, 2FYQA, 2HEKA, 2HHCA, 2IMFA, 2JE2A, 2JFRA, 2O4UX, 2O4VA, 2V3QA, 2VBMA, 2VLBC, 2VM9A, 2W3ZA, 2YXTB, 2ZAUA, 3B7NA, 3E9DA
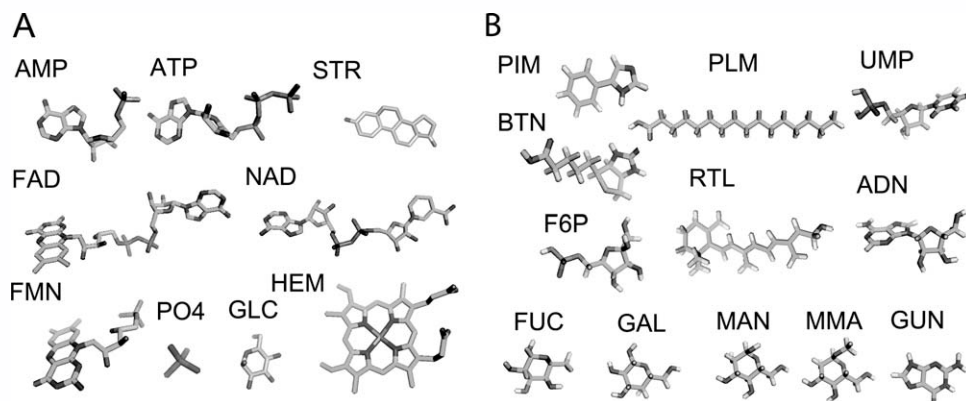
Figure 1
Ligand structures in the benchmark datasets. (**A**) Nine ligand structures in the Kahraman and the extended Kahraman dataset. (**B**) Twelve ligand structures in the Huang dataset. See text for the full spelling of the abbreviated molecular names.

Computing protein surface properties

The protein tertiary structure is represented by its surface shape. The surface of a protein is computed with the Adaptive Poisson–Boltzmann Solver (APBS) program,[35] which defines the surface as the boundaries of solvent accessible and solvent excluded regions. Surface shape information is stored in a 3D grid where grid points (voxel) that overlap with the protein surface are specified. For example, a 300 residue long protein fits into a 3D grid of the size 129 × 129 × 129 with a grid interval of 0.5 Å.

In addition to the geometrical shape, the protein surface is characterized with three other properties: the electrostatic potential, the hydrophobicity, and the visibility. These properties are assigned to each surface voxel. The electrostatic potential is computed with the APBS program, which solves the Poisson–Boltzmann equation. For the hydrophobicity, we use the Kyte–Doolittle hydrophobicity scale.[36] The Kyte–Doolittle hydrophobicity scale assigns a value between −4.5 (hydrophilic) and 4.5 (hydrophobic) to amino acid residues. To obtain the hydrophobicity of each voxel, first, each surface voxel is assigned with the hydrophobicity value of the closest

Table IC
The Ligand Pocket Benchmark Dataset From Huang et al.

Ligand molecule[a]	Average Size[a] (Å)	Average number of seed	Number of PDB entries	PDB entries[b]	Unbound structure[c]
AND	9.1	22.27	12	1bx4A, 1fmoE, 1mrgA, 1pg2A, 1vhwA, 2evaA, 2fqyA, 2pgfA, 2pkmA, 2zgwA, 3ce6A, 3fuuA	1ahcA
BTN	8.4	18.63	8	1bdoA, 1hxdA, 1stpA, 2b8gA, 2c4iA, 3d9lA, 3ew2A, 3g8cA	1swbA
F6P	8.7	19.8	10	1fbpA, 1lbyA, 1tipA, 1uxrA, 2cxsA, 2r66A, 3bxhA, 3h1yA, 3iv8A, 4pfkA	2fbpA
FUC (SAC)	6.7	8.63	8	1k12A, 1ivdB , 1lslA, 2a2qL, 2bs6A, 2j1tA, 2nzyA, 3cigA	1nnaA
GAL (SAC)	7.8	13.88	32	1gcaA, 1iszA, 1jz7A, 1kwkA, 1muqA, 1nsxA, 1okoA, 1r47A, 1rdk1, 1rvtJ, 1s5dD, 1tlgA, 1v3mA, 1w8nA, 1xc6A, 1z45A, 1zizA, 2b3fA, 2e9mA, 2ehnB, 2eukA, 2galA, 2j5zA, 2rjoA, 2v72A, 2vjjA, 2vnoB, 2zgnB, 3a23A, 3c69A, 3dh4A, 5abpA	1gcgA
GUN	8.1	14.64	10	1a95C, 1d6aA, 1it7A, 1sqlA, 1xe7A, 2i9uA, 2o74A, 2oodA, 2pucA, 3bp1B	1ulaA
MAN (SAC)	6.3	9.33	15	1apuE, 1bvwA, 1g12A, 1jndA, 1js8A, 1kdgA, 1kza1, 1m3yA, 1nhcA, 1qmoA, 1xxrB, 2duqA, 2e3bA, 3c6eC, 3d87D	3appA
MMA (SAC)	7.6	13	8	1kiuB, 1kwuA, 1lobA, 1msaA, 1s4pA, 2bv4A, 2g93A, 5cnaA	2ctvA
PIM	8.1	14	5	1e9xA, 1f4tA, 1s1fA, 1pdbA, 2d0tA	1phcA
PLM	9.0	28.3	24	1e7hA, 1eh5A, 1gxaA, 1hxs1, 1lv2A, 1m66A, 1mzmA, 1sz7A, 1u19A, 2debA, 2dt8A, 2e9lA, 2go3A, 2ifbA, 2jafA, 2nnjA, 2qztA, 2uwhA, 2w3yA, 2z73A, 3bfhA, 3bkrA, 3eglA, 3epyA	1ifbA
RTL	9.3	31.2	5	1fbmA, 1fmjA, 1gx8Am 1rbqA, 2rctA	1brqA
UMP	8.7	22.5	8	1bidA, 1f7nA, 1r2zA, 1sehA, 2bsyA, 2jarA, 2qchA, 3dl5A	3tmsA

[a]FUC, GAL, MAN, and MMA are also grouped as saccharide (SAC).
[b]Homologous structures to the unbound proteins are underlined, which are used to identify ligand-binding pockets of ligand unbound proteins. They are removed from the dataset when unbound structures are used as query.
[c]The unbound structures are used only for results in Table V.

amino acid residue, and then values are smoothed by averaging hydrophobicity values assigned to its neighboring surface voxels that are within two voxels apart. The surface visibility[31] indicates concaveness or convexness of a voxel. We defined the visibility of a voxel as the ratio of voxels occupied by the protein among the all the voxels within 5 Å to the target voxel. The visibility value ranges from 0 to 1.0 where 0 indicates the voxel is not close to a protein and 1 indicates that the voxel is completely buried in the protein. A large visibility value indicates that the voxel locates at a concave region of protein surface. As will be discussed later, the four properties of surface points are represented as the 3DZDs.

Pocket extraction by ray casting

The surface of a pocket region in the protein is extracted. The pocket surface is extracted by casting rays from the center of the ligand-binding pocket after the protein surface properties are computed. A pocket is defined as surface points that are encountered by rays cast from the ligand center position. If the position of a binding ligand is known, the center of mass of the ligand atoms is used to represent the center of the pocket location. In case the ligand-binding position is not known, the ligand-binding site prediction method, LIGSITE,[34] is used to predict the center of the binding pocket.

Local surface patch extraction

A pocket region is represented by a group of surface patches. A surface patch, which will be referred later simply as a "patch," is a connected single surface region within a specified distance (5–8 Å is tested) from a center point (voxel) called a "seed." The steps in seed selection are as follows: first, surface atoms of the selected pocket are determined as heavy atoms of residues within 3.5 Å to the pocket surface. Second, the first seed is selected from surface points that are closest to one of the surface atoms. Then the rest of seeds are determined by applying an iterative procedure of selecting a closest surface point for each of the surface atoms that is not closer than 3.0 Å to seed positions that are already selected. These steps distribute patches evenly on the pocket surface. On average there are 22.7 seeds (thus 22.7 patches) for a pocket.

Surface patch representation using the 3DZD

The four surface properties, the geometrical shape, the electrostatic potential, the hydrophobicity, and the visibility, mapped on a patch at the seed point x are considered as 3D grid functions, that is, $f_{shape}(x)$, $f_{ele}(x)$, $f_{hyd}(x)$, and $f_{vis}(x)$, respectively, which are represented by the 3DZD. The 3DZD allows compact and rotationally invariant representation of 3D objects (i.e., a 3D function).[32,37] Later,

we provide a brief mathematical derivation of the 3DZD. For more detail, see two previous studies of the 3DZD.[32,37] The 3DZD has also been successfully applied to various protein and ligand structure analyses,[23,38,39] including rapid protein global shape analysis (http://kiharalab.org/3d-surfer),[40,41] quantitative comparison for protein surface physicochemical properties,[42] small ligand molecule comparison,[43] protein–protein docking prediction,[44] and the comparison of low-resolution electron density maps.[45,46] In our previous works, we have shown that the 3DZD can also capture geometrical shape of local protein surfaces.[47,48]

A 3D function, $f(x)$, which contains a surface property of a patch, is expanded into a series in terms of Zernike–Canterakis basis[32] defined as follows:

$$Z_{nl}^m(r, \vartheta, \varphi) = R_{nl}(r) Y_l^m(\vartheta, \varphi) \qquad (1)$$

where $-1 < m < l$, $0 \leq l \leq n$, and $(n - l)$ even. $Y_l^m(\vartheta, \varphi)$, are the spherical harmonics and $R_{nl}(r)$ are radial functions constructed in a way that $Z_{nl}^m(r, \vartheta, \varphi)$ can be converted to polynomials in the Cartesian coordinates, $Z_{nl}^m(\mathbf{x})$. To obtain the 3DZD of $f(x)$, first, 3D Zernike moments are computed, which are defined by the expansion in this orthonormal basis:

$$\Omega_{nl}^m = \frac{3}{4\pi} \int_{|\mathbf{x}| \leq 1} f(\mathbf{x}) \bar{Z}_{nl}^m(\mathbf{x}) d\mathbf{x} \qquad (2)$$

Then, the 3DZD, F_{nl}, is computed as norms of vectors Ω_{nl}. The norm gives rotational invariance to the descriptor:

$$F_{nl} = \sqrt{\sum_{m=-l}^{m=l} (\Omega_{nl}^m)^2} \qquad (3)$$

The parameter n is called the order of 3DZD and it determines the resolution of the descriptor. n defines the range of l and a 3DZD is a series of invariants [Eq. (3)] for each pair of n and l, where n ranges from 0 to the specified order. We use order $n = 15$ (72 invariants) in the local surface patch comparison. Finally, the obtained 3DZD is normalized to a unit vector by dividing each moment by the norm of the whole descriptor. This normalization is found to reduce dependency of 3DZD on the number of voxels used to represent a protein.[42]

The 3DZD for the electrostatic potential, $f_{ele}(x)$, and the hydrophobicity, $f_{hyd}(x)$, are computed for voxels with a positive value and those with a negative value separately, and then concatenated to result in a vector of 72 × 2 = 144 invariants. This additional step is necessary to capture a spatial distribution of positive and negative values as we discussed in our previous work.[42] Thus, $f_{shape}(x)$ and $f_{vis}(x)$ are represented by a vector of 72
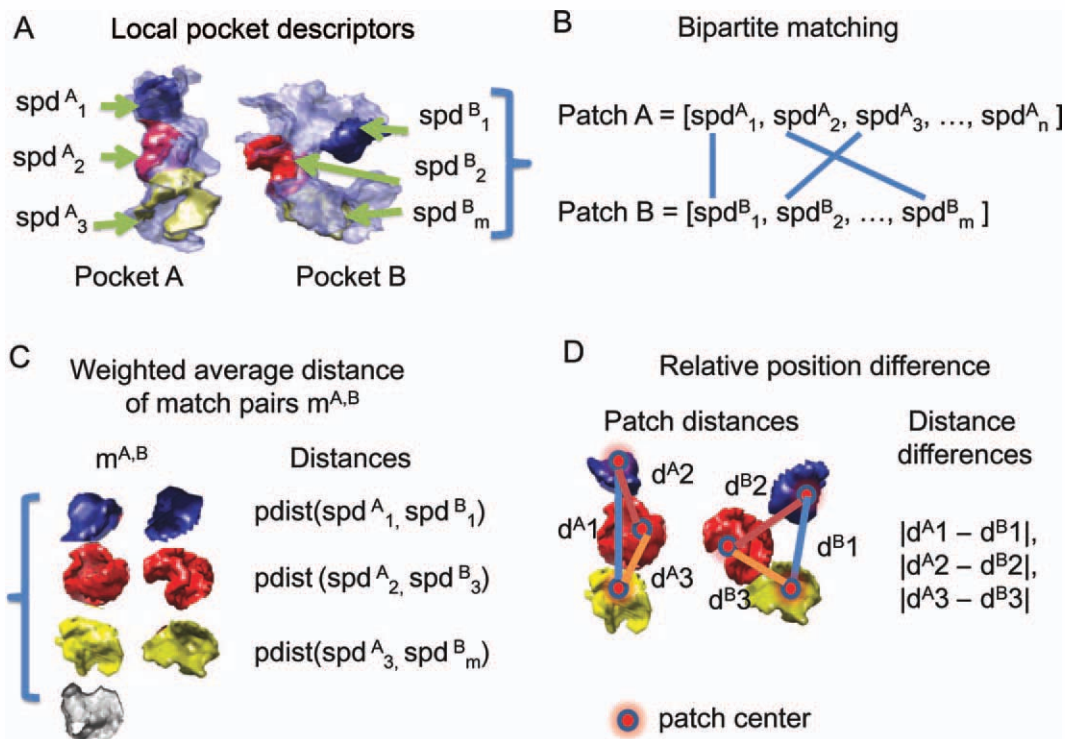
Figure 2

Illustration of surface patch descriptors and the comparison method used in Patch-Surfer. (**A**) Pocket descriptors that are composed of surface patch descriptors (*spds*). (**B**) The weighted bipartite matching algorithm. It matches pairs of surface patches from two pockets that have small distance defined by the score. (**C**) A scoring term for a pair of pockets considers the average of pairwise distance [Eq. (6)] of matched patches. (**D**) another scoring term compares mutual distance between patches in the two pockets [Eq. (7)].

invariant values while vectors for $f_{ele}(\boldsymbol{x})$ and $f_{hyd}(\boldsymbol{x})$ have 144 invariants.

Using the 3DZDs, a surface patch at the i-th seed of a pocket $\boldsymbol{P}$ is described by the surface patch descriptor $\boldsymbol{spd}_i^P$, which consists of the coordinate of the seed, $\boldsymbol{s}_i^P = (x_i^P, y_i^P, z_i^P)$, and normalized local 3DZDs, $\boldsymbol{lzd}_{i,shape}^P$, $\boldsymbol{lzd}_{i,hyd}^P$, $\boldsymbol{lzd}_{i,ele}^P$, and $\boldsymbol{lzd}_{i,vis}^P$, which are computed for the four features, shape, hydrophobicity, electrostatic potential, and visibility values that are mapped onto the surface points, $f_{shape}(\boldsymbol{x})$, $f_{ele}(\boldsymbol{x})$, $f_{hyd}(\boldsymbol{x})$, and $f_{vis}(\boldsymbol{x})$. A pocket P covered with n patches is represented as a set of the patches. Namely, $\boldsymbol{Pocket}(\boldsymbol{P}) = [\boldsymbol{spd}_1^P, \boldsymbol{spd}_2^P,\ldots, \boldsymbol{spd}_n^P]$. The pocket descriptor is illustrated in Figure 2(A).

Procedure of pocket comparison

The similarity of two pockets is quantified as a score that considers the distance of matched pairs of patches from the two pockets, the relative distance between the patches within each pocket, and the size of the pockets (Fig. 2). A query pocket A and a pocket B in a database are compared in the following three steps: (1) computing the distance of local surface patch pairs from the two pockets; (2) finding the corresponding matching pairs of

patches from pockets A to B; and (3) computing the overall distance score of the two pockets. Later, we explain each step of the procedure.

1. Computing the distance of all the pairs of surface patch descriptors from two pockets. The i-th patch from the query pocket A and the j-th patch from a database pocket B, $\boldsymbol{spd}_i^A$, and $\boldsymbol{spd}_j^B$, is computed as:

$$
p\text{dist}\left(\boldsymbol{spd}_i^A, \boldsymbol{spd}_j^B\right)
$$
$$
= \sum_{t\in\{shape,hyd,ele,vis\}} w_{j,t}^B \times L2\left(lzd_{i,t}^A, lzd_{j,t}^B\right), \quad (4)
$$

where $w_{j,t}^B$ are the weighting factor for each property type $t \in \{shape, hyd, ele, vis\}$ of the j-th patch of pocket B. $L2(lzd_{i,t}^A, lzd_{j,t}^B)$ is the L2 norm (the Euclidian distance) between two 3DZDs of the two patches of type t, $lzd_{i,t}^A$ and $lzd_{j,t}^B$. Thus, the patch distance is weighted sum of the distances between the 3DZDs of the four surface properties, shape, hydrophobicity, electrostatic potential, and visibility, which characterize the patches. The weighting factors in Eq. (4) are for normalizing the difference of the value distribution of the four properties. The weighting factors consider the average

(avg) and the standard deviation (std) of the Euclidian distance computed for 3DZDs of patches at the equivalent position in binding pockets of the same ligand type in the dataset. The weight for the feature t of the i-th patch in pocket P is defined as follows:

$$w_{i,t}^{P} = \frac{\frac{1}{(\text{avg}_{a(i),t} + 2*\text{std}_{a(i),t})}}{\sum_{s \in \{\text{shape,hyd,ele,vis}\}} \frac{1}{(\text{avg}_{\text{ALL},s} + 2*\text{std}_{\text{ALL},s})}} \quad (5)$$

$a(i)$ is the ligand atom where the seed of the i-th patch is closest to. Thus, $\text{avg}_{a(i),t}$ and $\text{std}_{a(i),t}$ is the average and the standard deviation of the Euclidean distances of 3DZDs of type t that are computed for patches locating at the same ligand atom $a(i)$ in the same ligand type. The average and the standard deviation are computed for pockets in the dataset, excluding the query pocket. $\text{avg}_{\text{ALL},s}$ and $\text{std}_{\text{ALL},s}$ are computed from all the patches of all ligand types in the dataset. For ligand-binding pockets that are not abundant in the dataset (STR in the Kahraman dataset), the overall average and the standard deviation values are used, which are computed for all the pairs of patches in all ligand-binding pockets in the dataset. Thus, $\text{avg}_{a(i),t}$ and $\text{std}_{a(i),t}$ in the numerator in Eq. (5) are replaced with $\text{avg}_{\text{ALL},t}$ and $\text{std}_{\text{ALL},t}$.

2. Finding matching patches from pockets A and B. Patches are matched so that the resulting matched patch pairs in the two pockets have the total minimum distance score. This problem is known as the weighted bipartite matching problem with only a difference being that our problem needs minimization of the score, whereas the original problem seeks for maximization of a score. The weighted bipartite matching problem can be approximately solved by the auction algorithm.[48,49] The distance score of each pair of patches is computed using Eq. (4). We introduced a distance threshold value to the original auction algorithm so that only similar patches are selectively paired, leaving dissimilar ones out from the matching. The bipartite matching is illustrated in Figure 2(B), and the detail of the modified auction algorithm is provided as Supporting Information Figure S1.

3. Computing the overall distance score of the two pockets. After surface patch matching is established, the overall score of the two pockets is computed using three terms, the weighted average distance score, a term for evaluating consistency of mutual position of matched patches, and the pocket size information. The average distance score of patches is defined as

$$\text{avg}Zd(A, B, \mathbf{m}^{A,B})$$
$$= \left(\frac{n_A}{N}\right)\left(\frac{1}{N}\sum_{i \in \mathbf{m}^{A,B}} p\text{dist}\left(\mathbf{spd}_{m_i^{A,B}}^{A}, \mathbf{spd}_{m_i^{A,B}}^{B}\right)\right), \quad (6)$$

where n_A is the number of patches in a pocket A, N is the number of pairs of patches from pockets A and B, and pdist is the distance score of two patches as defined in Eq. (5). $m^{A,B}$ contains the list of matched patch pairs from pockets A and B [Fig. 2(C)]. $m_i^{A,B}$ is the i-th matched patch pairs. n_A/N is a weighting factor for penalizing a match $m^{A,B}$ when the number of matched pairs (N) is smaller than the number of patches in the query, that is, pocket A (n_A).

The second term considers the relative position of matched patches in pockets A and B [Fig. 2(D)]. Relative position difference (*rpd*) of a match $m^{A,B}$ in pocket A and B is defined as

$$rpd(A, B, \mathbf{m}^{A,B}) = \left(\frac{n_A}{N}\right)$$
$$\times \left(\frac{2}{N(N-1)}\sum_{i=0}^{N-1}\sum_{j=i+1}^{N}\left|L2\left(\mathbf{s}_{m_i^{A,B}}^{A}, \mathbf{s}_{m_j^{A,B}}^{A}\right) - L2\left(\mathbf{s}_{m_i^{A,B}}^{B}, \mathbf{s}_{m_j^{A,B}}^{B}\right)\right|\right), \quad (7)$$

$\mathbf{s}_{m_i^{A,B}}^{A}$ is the coordinate of the seed point of the $m_i^{A,B}$-th patch in pocket A. Thus, the score computes the average of the difference of the Euclidean distance between the i-th and the j-th patches in pocket A and B.

The two terms are linearly combined to yield the pocket match distance (pocketMd) with weights w_1 and $1 - w_1$, where $0 \le w_1 \le 1$:

$$\text{pocket}Md(A, B, \mathbf{m}^{A,B}) = w_1 \times \text{avg}Zd(A, B, \mathbf{m}^{A,B})$$
$$+ (1 - w_1) \times rpd(A, B, \mathbf{m}^{A,B}) \quad (8)$$

In addition, we also considered the difference of the pocket size because they have been found to be effective in the previous studies[29,33]:

$$\text{pocket}Sd(A, B) = \left|\frac{n_A - n_B}{n_B}\right|. \quad (9)$$

Thus, it is computing the difference of the number of patches in the two pockets. The three terms are combined with another weighting factor, w_2 ($0 \le w_2 \le 1$), as follows:

$$\text{Totalscore}(A, B) = w_2 \times \text{pocket}Md(A, B, \mathbf{m}_{A,B})$$
$$+ (1 - w_2) \times \text{pocket}Sd(A, B) \quad (10)$$

The weight values of $w_1 = 0.3$ and $w_2 = 0.2$ are used in the study. These weights have been found to provide the best prediction rate on the Kahraman dataset using all the four surface properties and the pocket size score [Supporting Information Fig. S2(A)]. The second column of Table I lists the average pocket size. In Supporting Information Figure S2(B), we also show the average prediction success rate without using the weighting factor

n_A/N in Eqs. (6) and (7). By comparing Supporting Information Figure S2(A,B), it is shown that the inclusion of the n_A/N term increases the prediction success rates for majority of the weight combinations for w_1 and w_2. For example, for the weight combination $w_1 = 0.3$ and $w_2 = 0.2$ removing n_A/N deteriorates the average Top-1 success rate from 0.522 to 0.450, and Top-3 success rate from 0.824 to 0.814.

Ligand type prediction score

Pockets in the database are ranked in ascending order according to the distance to a query pocket using the scoring function [Eq. (10)]. Based on the ranked pockets, we use the following *Pocket_score* to predict the type of binding ligand molecules for the query pocket as proposed in our previous work.[29] Using the k closest pockets to the query, the score for a ligand type F for the query pocket P is defined as

$$\text{Pocket\_score}(P, F) = \sum_{i=1}^{k} \left(\delta_{l(i),F} \log\left(\frac{n}{i}\right) \right) \cdot \frac{\sum_{i=1}^{k} \delta_{l(i),F}}{\sum_{i=1}^{n} \delta_{l(i),F}},$$

(11)

where $l(i)$ denotes the ligand type (e.g., AMP, FAD, etc.) of the i-th closest pocket to the query, n is the number of pockets in the database, and the function $\delta_{l(i),F}$ equals to 1 if i-th pocket is of type F, and is 0 otherwise. The first term is to consider k closest pockets to the query, with a higher score assigned to a pocket with a higher rank. The second term is to normalize the score by the number of pockets of the same type F included in the database. The ligand with the highest *Pocket_score* is predicted to bind to the query pocket.

Performance evaluation of binding ligand prediction

Prediction performance is evaluated by the fraction of successful predictions where the correct ligand for the query pocket is predicted within top 1 or top 3 pocket scores. These are called the Top-1 and Top-3 success rate. We also use the area under curve (AUC) of the receiver operating characteristic (ROC) curve. To obtain the ROC curve, the k closest pockets in the database to the query are retrieved. Then they are evaluated by computing false positive (x-axis) and true positive (y-axis) rate at different score cutoff values. The value of k is varied from 1 to N where N is the number of pockets in the dataset. The false positive rate is defined as the ratio of the number of retrieved pockets of different ligands to the query (i.e., false positives) relative to the total number of pockets of different ligands the dataset. The true positive rate is the ratio of the number of correctly retrieved pockets of the same ligand type relative to the total number of pockets of the same type in the dataset. The false positive rate equals true positive rate, on average, in random retrieval, which yields an AUC value of 0.5.

RESULTS

Variance of properties of ligand-binding pockets

To begin with, we examined the variation of properties of pockets in the Kahraman dataset and the Huang dataset. Figure 3 shows the mapping of average Euclidian distances of 3DZDs of surface patches that are grouped and mapped according to the closest ligand atom. The maps are computed for the four properties, the shape, the hydrophobicity, the electrostatic potential, and the visibility. The figure shows different ligand-binding pockets have different levels of conservation of the properties. FUC is relatively well conserved in all four properties, whereas RTL binding pockets show a large variation in all the properties at the alcohol group at the end of the poly unsaturated side-chain (the right side of RTL in Fig. 3). In addition, the conserved regions can be different for the different properties. For example, PO4-binding region is the most conserved region in the ATP-binding pockets in terms of the hydrophobicity (green), whereas the same region is not well conserved in terms of the other properties, especially for the electrostatics potential and the visibility. The observed diversity of the different properties at equivalent position in binding pockets has motivated us to segment pocket surface into local patches so that the comparison can accommodate the difference in the surface properties within the pockets.

Retrieval performance of Pocket-Surfer and Patch-Surfer

Next, we examine overall pocket retrieval performance of the Patch-Surfer and Pocket-Surfer using surface shape and size information on the Kahraman dataset and the Huang dataset. The resulting ROC curves are shown in Figure 4. The performance was compared with and without pocket size information for both methods. More concretely, Eq. (8) was used for considering pocket shape, whereas Eqs. (9) and (10) were used for encoding shape and the size information for Patch-Surfer. As the pocket size information, the average number of seeds in pockets was used (Table IA for the Kahraman data set and Table IC for the Huang dataset). The number of seeds correlates well with the molecular mass of the ligand molecules with the correlation coefficient of 0.994. For Pocket-Surfer, the average distance from the center of a pocket to the pocket surface is used following our previous work[29] (Tables IA and IC). As described in Materials
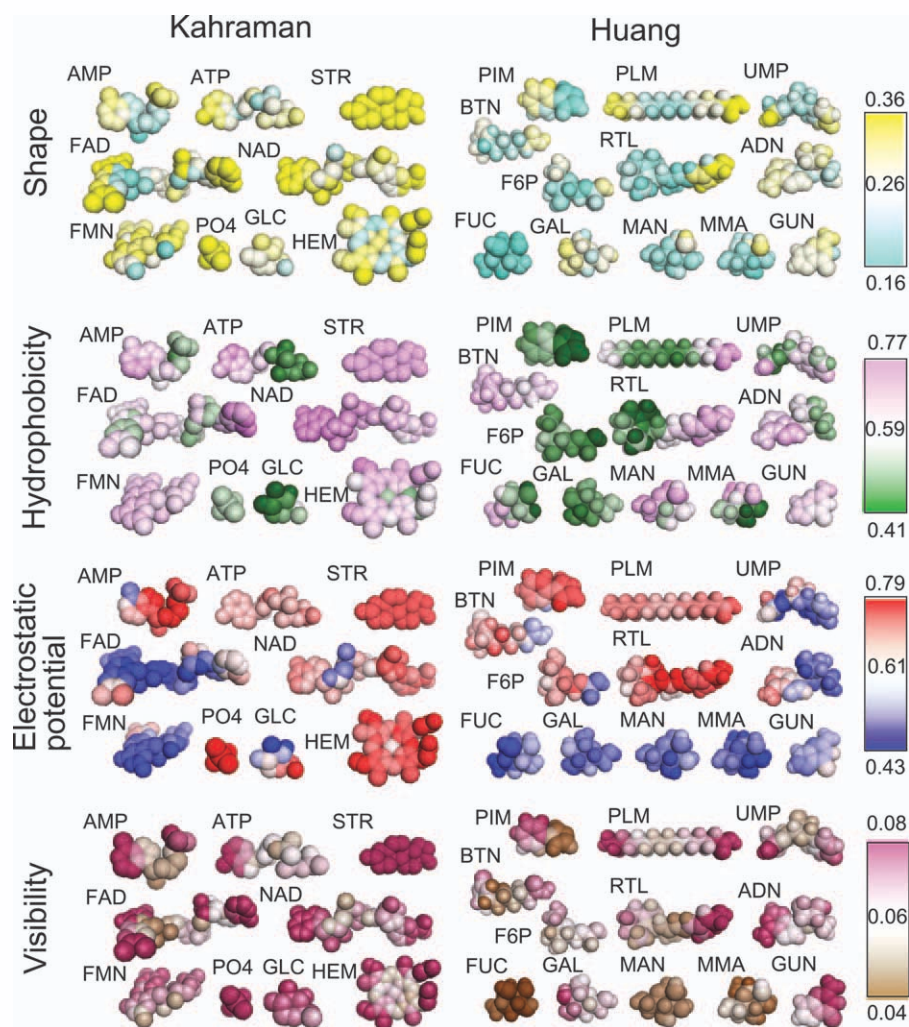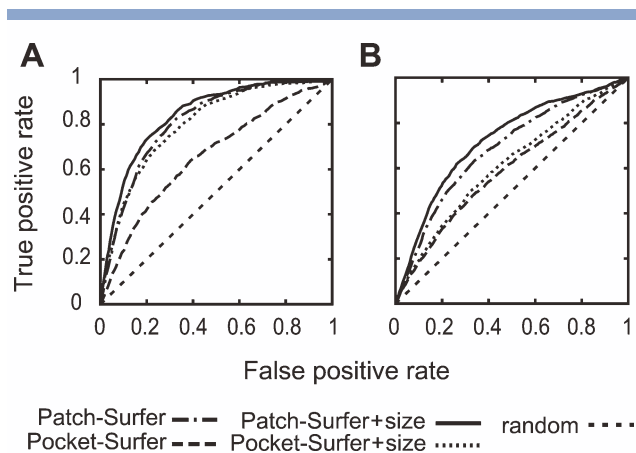
Figure 3

Average 3DZD distance of four properties used to characterize pockets. The average distance of 3DZDs of patches at equivalent position in pockets is computed and mapped to the closest ligand atoms. The distance is shown in color, from cold color (smaller distance) to warm color (larger distance). The first row shows distances of surface patch shape. Second row shows the hydrophobicity. The third row shows the electrostatic potential. The last row shows the visibility. The ranges of color codes shown in the bars are average distance plus/minus two times of the standard deviation. For STR, the average distance of all patch pairs in the pockets are mapped to all the atoms because there are not many structures available for meaningful statistics (three EST and two AND).

and Methods, Patch-Surfer uses the weighting factors $w_{i,\text{shape}}^{p}$ [Eq. (5)] to balance contribution of each patch at a different position in the overall score. For the results shown in Figure 4, we conducted a leave-one-out procedure, that is, the query pocket is excluded when the average and standard deviation of the Euclidian distance of the 3DZDs were computed to obtain the weighting factor values.

It is shown that Patch-Surfer outperforms Pocket-Surfer with and without pocket size information (Fig. 4 and Table II). For the both datasets, Patch-Surfer using pocket size information performed the best followed by Patch-Surfer without pocket size. Table II summarizes

the ROC AUC values of the two methods along with four similar pocket descriptors reported in previous work.[29] Legendre moments, 2D Zernike moments, and 2D pseudo-Zernike moments are two-dimensional shape descriptors, which encode two-dimensional projections of pockets that describe the distance of the pocket wall from the pocket center. The results of spherical harmonic method are taken from Kahraman et al.[33] The four descriptors are global descriptors of pockets, which are the same as Pocket-Surfer. Among these descriptors, Patch-Surfer clearly outperforms the others. Note that Pocket-Surfer was previously[29,39] shown to outperform four other existing methods, eF-Seek,[24] SitesBase,[50]

Figure 4

ROC curves of Pocket-Surfer and Patch-Surfer using the shape and the size information. (**A**) The Kharaman dataset. (**B**) The Huang dataset. The AUC values of the curves are shown in Table II. The patch radius was set to 5 Å. A random retrieval yields the AUC of 0.5.

PROSURFER,[51] and XBsite2F[52]; and here we show that Patch-Surfer performs even better than Pocket-Surfer.

Patch-Surfer and Pocket-Surfer with/without size information showed better retrieval performance on the Kahraman dataset than the Huang dataset. One of the reasons for poorer performance on the Huang dataset is that they are composed of similar sized pockets for smaller ligand molecules. Pockets in the Kahraman dataset have an average of 22.5 seed points with standard deviation of 11.0, whereas the Huang dataset has an average of 18.0 seeds with the standard deviation of 7.1. In addition, the Huang dataset includes pockets with ligand molecules with similar chemical structures, that is, FUC, GAL, MAN, and MMA, which are all single ring sugar molecules and were not well distinguished between each other, as we will show later.

Parameter optimization on the Kahraman dataset

In the previous section, we demonstrated that Patch-Surfer performs the best among the related pocket descriptors (Table II and Fig. 4). Here, we examine prediction performance of Patch-Surfer with different patch sizes and different combinations of surface properties (Table III). The binding ligand type prediction was made by considering the top 18 [$k = 18$ in Eq. (11)] retrieved pockets. $k = 18$ was found to provide the best average prediction rate (Supporting Information Fig. S3). Eighteen is twice the number of ligand types included in the Kahraman dataset.

As consistent with Figure 4, adding the pocket size information improved the prediction rate for all the combinations of properties and the patch sizes tested. For example, when the pocket size information was not used, the average Top-3 success rate by using pocket shape information only (S - - -) was 0.752, which was improved to 0.867 when the pocket size information was combined. As for the patch size, four different radii, 5.0, 6.0, 7.0, and 8.0 Å were tested. We observe a moderate trend that a smaller patch size performed better for Top-1 prediction success rate, whereas larger patch sizes showed better performance for the Top-3 success rate on average. Adding more terms did not simply improve the success rate. Using all the four properties Patch-Surfer with shape, the hydrophobicity, the electrostatic potential, and the visibility (SHEV) performed best on average with the pocket size in terms of the Top-1 success rate (0.473). On the other hand, using only the shape information (S - - -) showed the highest average Top-3 success rate with the pocket size information (0.867). Overall, we did not observe a single best combination of the properties that consistently performed better than the others. This observation is somewhat consistent with a previous work,[26] which reports that combining the electrostatic potential to the size information did not make consistent improvement of pocket retrieval accuracy. This may be due to the diverse nature of property conservation of ligand-binding pockets as we have seen in Figure 3.

In the following sections, we will provide results of using the patch radius of 5.0 Å, which showed the highest average prediction rate of 0.414 for the Top-1 prediction and the second best prediction rate (0.797) when the Top-3 predictions considered. As for the property combinations, we use the shape only (S - - -) and all four properties (SHEV). These two combinations had the two highest average Top-1 prediction rate over the four different patch radii, 0.471 and 0.473 respectively, when the pocket size information was used.

Prediction results of individual ligand types in the Kahraman Dataset

Figure 5 shows the breakdown of prediction accuracy for individual ligand types in the Kahraman dataset. The

Table II

Average Area Under ROC Curve for Different Methods

Methods	Kahraman dataset		Huang dataset	
	Shape	Shape + size	Shape	Shape + size
Patch-Surfer	0.81	0.84	0.64	0.68
Pocket-Surfer (3DZD)[a]	0.66	0.81	0.54	0.63
Legendre[a]	0.53	0.77	—	—
Pseudo-Zernike[a]	0.66	0.79	—	—
2D Zernike[a]	0.66	0.78	—	—
Spherical harmonics[b]	0.64	0.77	—	—
Random	0.5	0.5	0.5	0.5

[a]The results are taken from our previous work (Ref. 29).
[b]The results are taken from Kahraman et al.[33] The results for the Huang dataset are not available because it was not used in their article.

Table III
The Success Rate of Binding Ligand Prediction on the Kahraman Dataset Using Different Parameters

Score combination		Top-1 prediction success rate					Top-3 prediction success rate				
Properties used[a]		PR[b] 5 Å	PR 6 Å	PR 7 Å	PR 8 Å	Avg.[c]	PR 5 Å	PR 6 Å	PR 7 Å	PR 8 Å	Avg.[c]
Without pocket size	S − − −	0.382	0.338	0.315	0.315	0.338	0.754	0.693	0.780	0.780	0.752
	S − −V	0.383	0.333	0.364	0.364	0.361	0.739	0.732	0.775	0.775	0.755
	S−EV	0.371	0.392	0.383	0.383	0.382	0.764	0.744	0.749	0.749	0.752
	SH−V	0.306	0.350	0.337	0.337	0.333	0.742	0.705	0.786	0.786	0.755
	SHEV	0.382	0.322	0.350	0.350	0.351	0.729	0.730	0.685	0.685	0.707
With pocket size	S − − −	0.483	0.478	0.461	0.461	0.471	0.840	0.851	0.888	0.888	0.867
	S − −V	0.470	0.462	0.444	0.444	0.455	0.843	0.848	0.866	0.866	0.856
	S−EV	0.480	0.486	0.436	0.436	0.460	0.848	0.848	0.843	0.843	0.846
	SH−V	0.432	0.460	0.442	0.442	0.444	0.837	0.866	0.803	0.803	0.827
	SHEV	0.455	0.463	0.486	0.486	0.473	0.870	0.829	0.848	0.848	0.849
Average		0.414	0.408	0.402	0.402	0.407	0.797	0.785	0.802	0.802	0.797

[a]Combination of the properties used for prediction are shown. The shape (S), the hydrophobicity (H), the electrostatic potential (E), and the visibility (V).
[b]The patch radius (PR) of the sphere used to define patch regions.
[c]Average over different patch sizes.

performance of Patch-Surfer are analyzed using the two property sets, the shape only (S - - -) and all four properties, that is, SHEV with and without pocket size information. For comparison, retrieval results for Pocket-Surfer are shown along with the results for Patch-Surfer using only the pocket size information and the result of random retrieval. In each panel in Figure 5, the first three bars from the left show the results without using the pocket size information, whereas the next three bars

are the results using the pocket size information by Pocket-Surfer, Patch-Surfer (S - - -), and Patch-Surfer (SHEV), respectively.

By observing the average performance over different ligand types (Figure 5, bottom right panel), both Pocket-Surfer and Patch-Surfer showed a Top-3 success rate of over 0.80. Clearly, both Pocket-Surfer and Patch-Surfer performed better than size information alone or random retrieval. Patch-Surfer with the shape information only (S - - -)
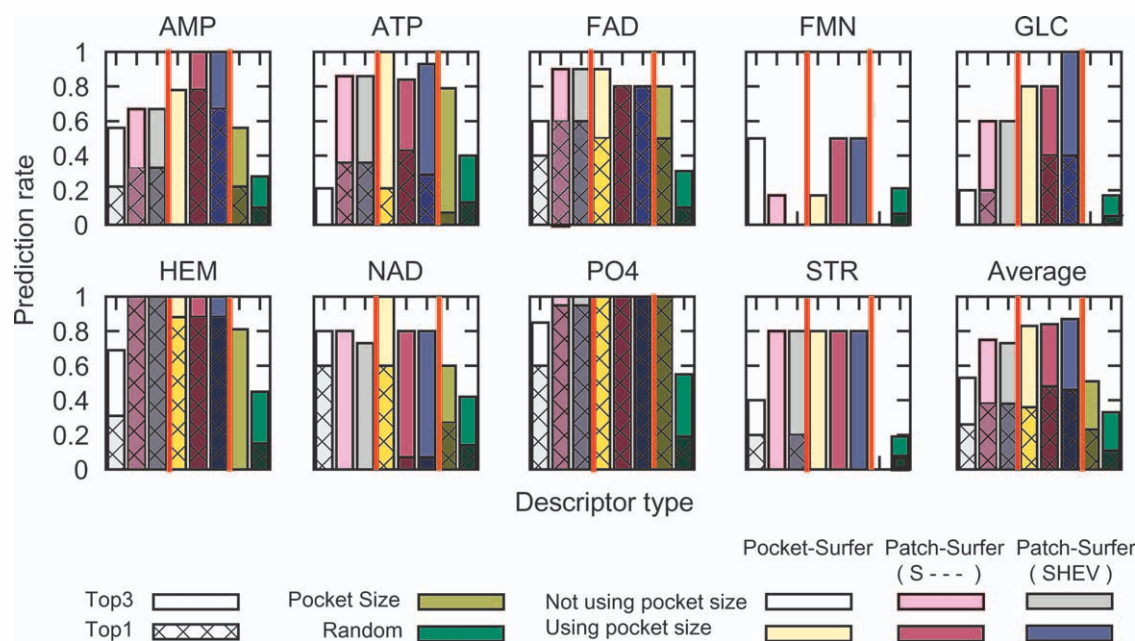
Figure 5
Prediction success rates for each ligand type in the Kahraman dataset. For each ligand type, the first three bars from the left show the results without using the pocket size information, whereas the next three bars are results with the pocket size information. Three bars are the results of Pocket-Surfer, Patch-Surfer with shape information (S - - -), SHEV information, from left to right. The bar in olive (the second one from right) shows the retrieval results using the pocket size information only. The rightmost bar is the results of a random retrieval. The cross-hatched bars show the Top-1 success rate and the solid bars show the Top-3 success rate.
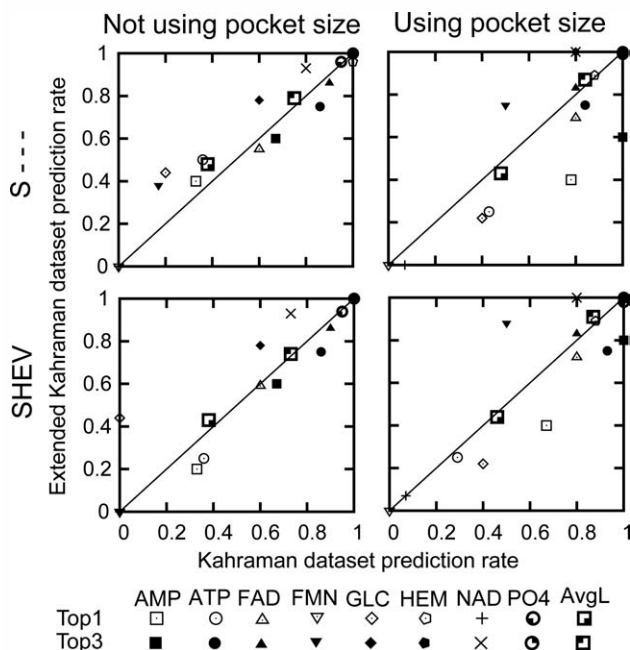
Figure 6

Comparison of the prediction success rate by Patch-Surfer for the original and the extended Kahraman dataset. The Top-1 and Top-3 success rates of individual ligand types as well as the average success rate over all the ligands are compared. (**A**) Only shape property was used (S - - -); (**B**) the shape property was used in the combination with the pocket size infromation; (**C**) the shape, the hydrophobicity, the electrostatic potential and the visibility properties (SHEV) were used; (**D**) the four properties (SHEV) were used with the size information.

outperformed over the Pocket-Surfer for both with and without pocket size. Using the pocket size information improved the prediction rates for both Pocket-Surfer and Patch-Surfer by 0.08–0.20. The best Top-3 success rate, 0.87, was achieved by Patch-Surfer using all four properties (SHEV) and pocket size information.

When assessing the prediction success rate of individual ligand types, the prediction success rate differs from ligand to ligand. For example, the Top-3 success rate by Patch-Surfer using the four properties and the pocket size (purple bars) ranged from 0.50 for FMN to 1.00 for AMP, GLC, HEM, and PO4. When only the surface shape property was used without the pocket size information (the two leftmost bars in each panel), Patch-Surfer showed better Top-3 success rate than Pocket-Surfer in seven out of nine ligand cases (two exceptions are FMN for which Pocket-surfer showed better results and NAD for which had tied performance), indicating that patches used in Patch-Surfer effectively captured the local geometrical similarity of ligand-binding pockets. The prediction accuracy of the PO4-binding pockets was perfect (1.0) even when only the pocket size was used due to its distinctively smaller pocket size (Table IA).

Evaluation of the transferability of parameters

Next, we benchmark Patch-Surfer on the extended Kahraman dataset (Table IB), which contains different sets of proteins that bind the same ligand molecules as the original Kahraman dataset. This dataset was used to examine how well the parameters determined with the original Kahraman dataset perform for unseen proteins. Figure 6 and Table IV compares the prediction success rates of Patch-Surfer on the original Kahraman set (*x*-axis) and the extended Kahraman set (*y*-axis) using the combination of with/without pocket size information and shape only (S - - -) or all four properties (SHEV).

It is shown that the prediction performance for the two datasets is comparable. Moreover, results from the extended dataset were often better than those from the original dataset. Concretely, the Top-3 average success rate on the extended dataset was better than the original dataset for all the cases [Fig. 6(A–D) and Table IV]. Looking at the results for individual ligand types, several ligands have lower Top-1 success rate in the extended dataset when the pocket size information is used [Fig. 6(B,D)]. However, on average the Top-1 success rate was also comparable between the original and the extended datasets. Without pocket size information, the Top-1 success rate was larger for the extended dataset [Fig 6(A,C)]. When the pocket size information is combined [Fig. 6(B,D)], the Top-1 success rate of the extended dataset was lower than that of the original dataset, but the difference was marginal (Table IV). We conclude that the weighting factor values trained on the original dataset can be applied to other proteins, which are not homologous to proteins in the original dataset.
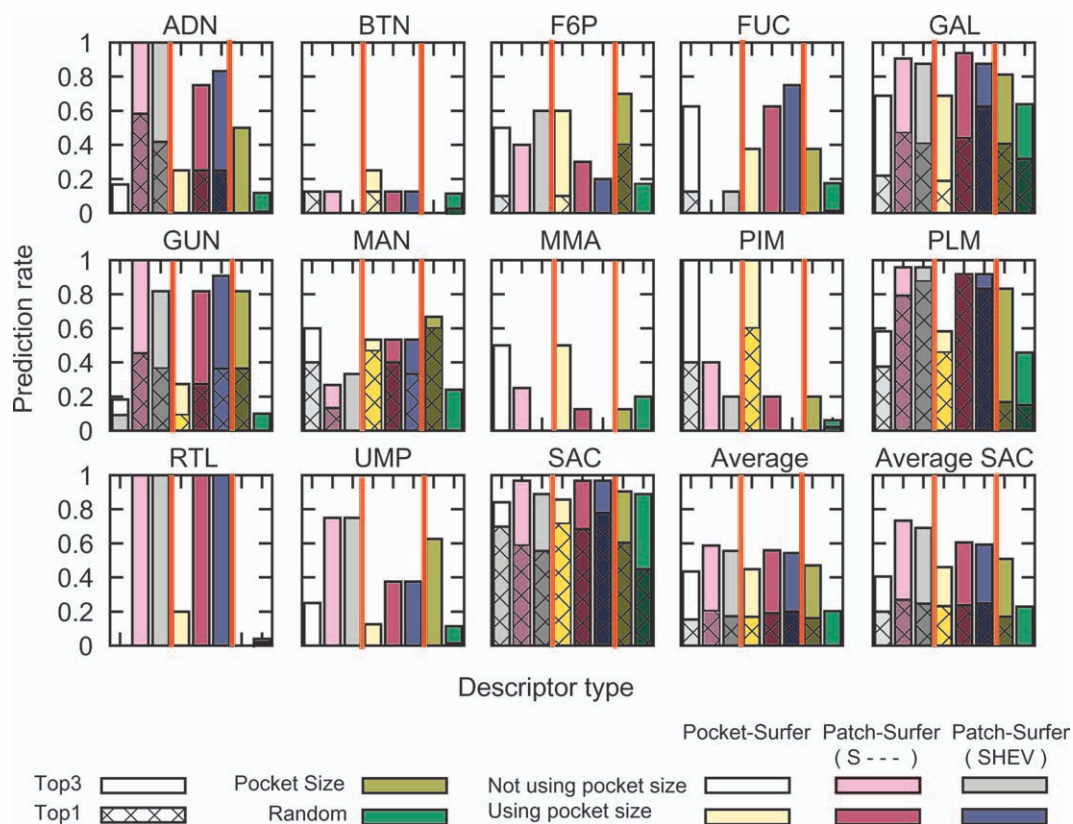
Ligand Prediction on the Huang Dataset

We further examine the prediction performance of Patch-Surfer and Patch-Surfer on the Huang dataset, which contains 12 different ligand types to those of the Kahraman dataset (Fig. 7). Again, Patch-Surfer shows overall higher Top-1 and Top-3 accuracy when compared with Pocket-Surfer (the "average" panel at the bottom right). We find that ligand types that were better predicted with Patch-Surfer, ADN, PLM, RTL, and UMP, are relatively larger and more flexible, which are difficult for

Table IV

Summary of Prediction on the Original and the Extended Kahraman Datasets

| | Not using pocket size | | | | Using pocket size | | | |
| | S − − − | | SHEV | | S − − − | | SHEV | |
Descriptor	Top1	Top3	Top1	Top3	Top1	Top3	Top1	Top3
Original Kahraman	0.38	0.75	0.38	0.73	0.48	0.84	0.46	0.87
Extended Kahraman	0.48	0.79	0.43	0.74	0.43	0.87	0.44	0.91

Figure 7

Binding ligand prediction on the Huang dataset. The Top-1 and Top-3 prediction success rate for each ligand types as well as the average values on the Huang dataset by Pocket-Surfer and Patch-Surfer are shown. The ligand group SAC composes of FUC, GAL, MAM, and MMA. "average SAC" considers FUC, GAL, MAM, and MMA as a single ligand type. See Figure 5 for more details.

Pocket-Surfer (Fig. 3). In addition, GAL and GUN are two small ligands for which Patch-Surfer performed better than Pocket-Surfer.

Patch-Surfer did not show improved performance over Pocket-Surfer for some of small pockets whose shape is well conserved. For example, pockets of BTN are consistent in shape, and have no strongly conserved region of hydrobicity, electrostatic potential and visibility. In addition, FUC, MAN, MMA, each has a low prediction success rate by both methods due to their high mutual similarity. In fact, these ligands are known to interchangeably bind to the same protein pockets. For example, GAL and MMA bind to the same pocket in the lactoferrin crystal structures (PDB ID: 2dqvA and 2g93A). Similarly, MAN and MMA bind to the same location in lectin (1rinA and 1lobA). In addition, a crystal structure of human EPHB2 receptor (1b4fA) binds MAN and FUC at the same pocket whereas a crystal structure of glutathione synthetase (1gltA) has FUC and GAL binding in the same location. Considering the similarity of these four ligands, we also examined the success rate by grouping these ligands into a single group, saccharides (SAC). The success rate for SAC was very high (panel named

"SAC" in the bottom row) for both Patch-Surfer and Pocket-Surfer, which also made an improvement on the overall average prediction success rate ("average SAC" panel).

Effect of the ligand flexibility to prediction accuracy

Because one of the motivations of developing Patch-Surfer is to better handle pockets for flexible ligand molecules, we examined how much the flexibility of ligands affect to the retrieval accuracy. In Figure 8, the difference in the rank of the top ranking correct binding site by Pocket-Surfer and Patch-Surfer for each query pocket (y-axis) is plotted relative to the RMSD of ligand pairs (x-axis). The y-axis shows the rank of a binding pocket by Pocket-Surfer minus the rank by Patch-Surfer; thus, positive values indicate superior performance by Patch-Surfer. Overall, on both Kahraman and Huang datasets, Patch-Surfer retrieved binding sites of the same type as query at a lower rank than Pocket-Surfer except for some ligand types [e.g., NAD in the Kahraman dataset, Fig. 8(A,B); MAN in the Huang dataset, Fig. 8(C,D)]. The advantage
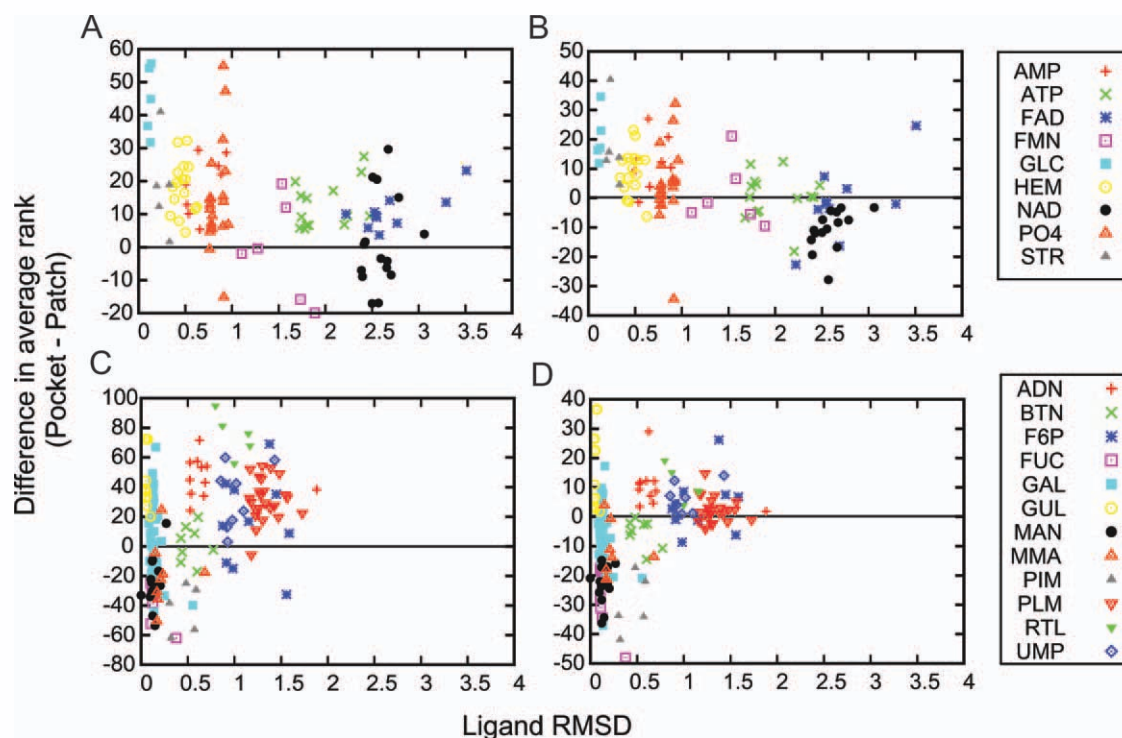
Figure 8

The ligand RMSD and the retrieval rank difference by Pocket-Surfer and Patch-Surfer. The *x*-axis shows the average RMSD between the ligand molecule of each query pocket to the other ligands of the same type in the dataset. The *y*-axis shows the difference in the retrieval rank of each ligand of the same type by Pocket-Surfer and by Patch-Surfer (rank by Pocket-Surfer–rank by Patch-Surfer). (**A**) and (**B**) results on the Kahraman dataset using pocket shape information with and without using pocket size information, respectively. (**C**) and (**D**) are results on the Huang dataset. Retrieval was performed using pocket shape information (C), without and (D), with pocket size information.

of Patch-Surfer is more obvious when the pocket size information was not combined [Fig. 8(A,C)]. On the Kahraman dataset, Patch-Surfer shows large improvement in retrieving for flexible ligands, ATP, and FAD, for which many pairs have an RMSD higher than 2 Å [Fig. 8(A)]. In the Huang dataset, Patch-Surfer showed improved retrieval ranks for two of the most flexible ligands, F6P, and PLM, especially when the size information is not used [Fig. 8(C)].

Effect of global structural similarity to the retrieval performance

Next, we examine how much the global structure similarity of a query protein to proteins in the database affect to the retrieval (Fig. 9). For both Kahraman [Fig. 9(A,B)] and the Huang dataset [Fig. 9(C,D)], no correlation was observed between the global RMSD (*x*-axis) of the protein structure and the rank of the retrieved pocket. Thus, Patch-Surfer is able to identify binding pockets of the same ligand type even if the global structure of the proteins is very different. This is advantageous in annotating function of proteins that do not have apparent sequence and structure similarity to proteins of known function.

Examples of pocket matching

In this section, we provide several examples that illustrate how similar patches in pockets are matched by Patch-Surfer. In these examples, all four surface properties were used to define the similarity of the patches. Figure 10 shows pairs of binding pockets of the same ligand type that have different overall pocket shape due to the flexibility of binding ligands. For these pockets, Patch-Surfer retrieved them at higher ranks than Pocket-Surfer by correctly identifying the corresponding surface patches. The first example is a pair of FAD binding proteins [Fig. 10(A)]. In the crystal structure of flavohemoglogin (1cqx, left), the bound FAD is bound in a stretched form. On the other hand, rotatable bonds of the PO4 groups in the middle of FAD have different angles when bound to thiol oxidase (1jr8, right), which induces the change in conformation of FAD and thus causing the overall binding pocket shape to be very different from 1cqx. The apparent difference in the overall shape between the two pockets made it difficult for Pocket-Surfer to retrieve the correct pocket when queried by the other (1jr8 was retrieved for a query 1cqx that was ranked 21st by Pocket-Surfer). In contrast, Patch-
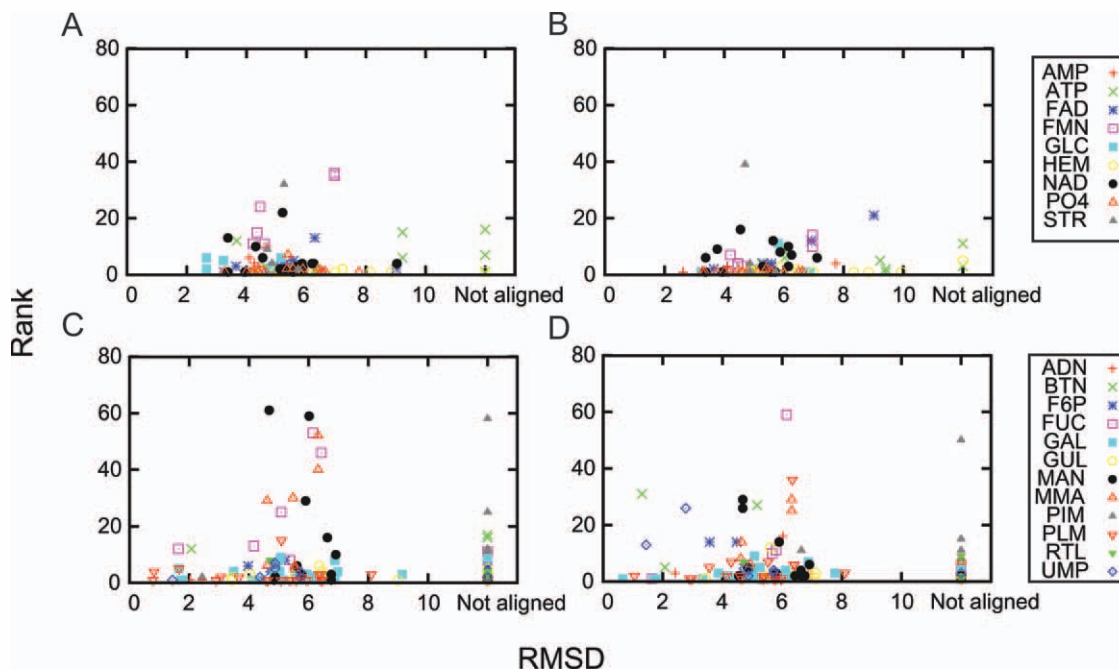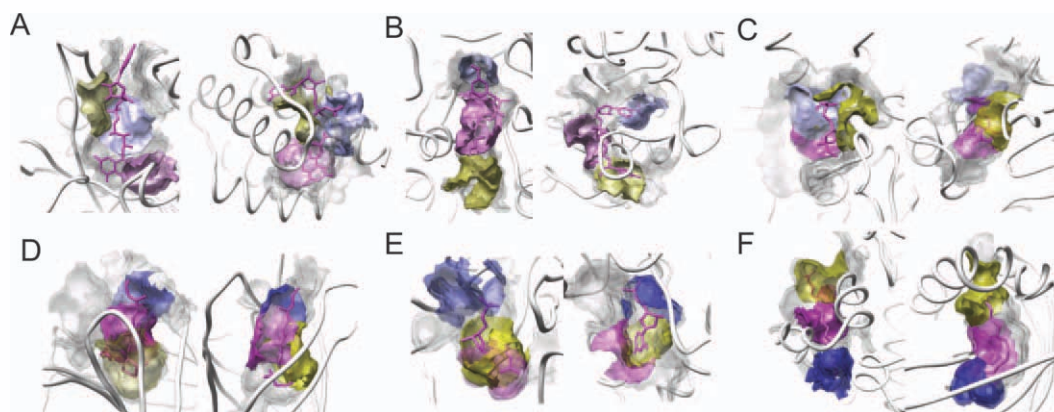
Figure 9

The RMSD of the global structure of proteins and the rank of the pockets retrieved by Patch-Surfer. For each query pocket, the best rank among the pockets of the same ligand type plotted (*y*-axis) relative to the global RMSD of the proteins (*x*-axis). The Combinatorial Extension (CE) program[53] was used to compute the RMSD. Points at the rightmost bar are proteins that CE could not structurally align to the query protein because their structures are overly different. Results for the Kahraman dataset is shown in (**A**) using the shape information only; (**B**) using the shape combine with the size information. Result for the Huang dataset is shown in (**C**) using the shape only; and (**D**) using the shape and the size information.

Surfer managed to retrieve 1jr8 as the fourth rank by identifying equivalent patches in the two pockets. In the figures, pairs of identified corresponding patches in the two pockets are shown in the same color. The next example is NAD-binding pockets [Fig. 10(B)]. Similar to the previous example, NAD binds to the two pockets with

Figure 10

Examples of pocket matching by Patch-Surfer. A query pocket is shown in left and a pocket retrieved from the dataset is shown on the right hand side. (**A**) A pair of proteins that bind FAD, 1cqx (left) and 1jr8 (right). The RMSD of two FAD is 3.79Å. (**B**) A pair of NAD-binding proteins, 1mi3 (left) and 1s7g (right). The RMSD of the ligand molecules is 3.49 Å. (**C**) A pair of F6P-binding proteins, 2r66 (left) and 3bxh (right). The RMSD of the ligands is 1.02 Å. (**D**) A pair of RTL-binding proteins, 1gx8 (left) and 1rbp (right) where the ligand RMSD is 0.90 Å. (**E**) A pair of UMP-binding proteins, 2qch (left) and 2jar (right) where the ligand RMSD is 1.45Å. (**F**) A pair of PLM-binding proteins, 2nnj (left) and 2w3y (right) where the ligand RMSD is 1.34 Å. Matching pairs of local patches for each of the pairs of proteins are shown. Color codes indicate corresponding matched patches from two proteins.
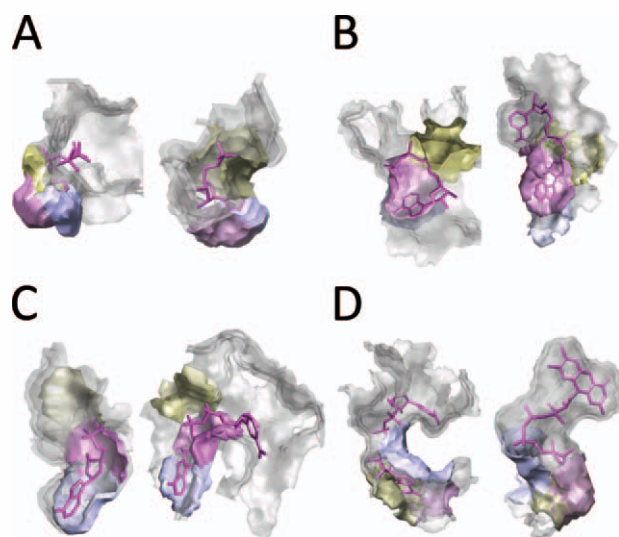
Figure 11

Examples of pairs of pockets for ligands with the same chemical group whose same moiety regions were matched by Patch-Surfer. (**A**) 1b8a (ATP binding) in left and 1kht (AMP) in right. (**B**) 1dy3 (ATP) in left and 1tox (NAD) in right. (**C**) 1s7g (NAD) in left and 1k87 (FAD) in right. (**D**) FMN-binding protein 1kht (left) and FAD-binding protein 1pox (right).

very different conformation (the RMSD of the two NAD in 1mi3 and 1s7g is 3.49 Å). A NAD-binding protein, 1s7g, was ranked as 3rd by Patch-Surfer and as the 9th by Pocket-Surfer, when queried using 1mi3. Figure 10(C–F) shows four more examples of the same ligand type binding pockets that are retrieved with a higher rank by Patch-Surfer than Pocket-Surfer. A protein with a F6P-binding pocket, 3bxh, was ranked fourth by Patch-Surfer, whereas ranked 26th by Pocket-Surfer when queried using 2r66 [Fig. 10(C)]. Similarly, the pair of RTL-binding proteins, 1rbp was ranked 9th and 38th by Patch-Surfer and Pocket-Surfer respectively, when queried using 1gx8 [Fig. 10(D)]. A UMP-binding proteins, 2jar, was retrieved at the 3rd rank and the 27th [Fig. 10(E)] by Patch-Surfer and the Pocket-Surfer respectively, using 2qch as the query. A PLM-binding proteins, 2w3y, was ranked 3rd by Patch-Surfer, whereas ranked 28th by Pocket-Surfer when queried using 2nnj [Fig. 10(F)].

The previous examples shown in Figure 10 demonstrate that Patch-Surfer is more tolerant to the conformational differences in the binding pockets. However, the patch representation of pockets sometimes does not contribute to improvement of the binding ligand prediction accuracy, rather in the opposite way. The main cause of this is attributed to the shared chemical groups between ligand molecules, in which local binding surfaces are recognized as similar patches by Patch-Surfer. Figure 11 shows several of such examples. AMP, ATP, FAD, and NAD contain adenosine [Fig. 11(A–D)]. Binding surfaces

of the adenosine moiety of these molecules are identified as similar patches by Patch-Surfer, which often makes Patch-Surfer retrieve them at high ranks when queried by each other. Figure 11(A) is a pair of ATP-binding (left, 1b8a) and AMP-binding (right, 1kht) pockets. The obvious chemical similarity of binding pockets of these two molecules was identified by Patch-Surfer. When the original Kharaman dataset was searched from 1b8a, 1kht was ranked at the top, whereas Pocket-Surfer ranked it at 13th. In the next example [Fig. 11(B)], an ATP-binding pocket (left, 1dy3) was ranked at the 2nd when queried using a NAD-binding pocket (right, 1tox) by Patch-Surfer (Pocket-Surfer ranked it at 43rd). Figure 11(C) is a pair of pockets that bind NAD (left, 1s7g) and FAD (1k87), which also have the adenine group. The retrieved rank of 1k87 queried from 1s7g was the 4th by Patch-Surfer and the 17th by Pocket-Surfer. The last panel [Fig. 11(D)] shows the binding pockets of FMN and FAD, both of which contain flavin. Pocket-Surfer recognized the difference of the overall shape of the two pockets, ranking 1ja1 (the FMN-binding pocket) at the 47th when queried from 1pox (FAD-binding pocket). On the other hand, Patch-Surfer ranked 1ja1 higher at 12th due to the recognition of the similarity in flavin-binding patches of the two pockets.

The recognition of binding regions of chemical groups does not always contribute to improvement in the prediction accuracy of binding ligands; however, it suggests that Patch-Surfer can be developed into a unique method for predicting chemical group binding sites rather than predicting the entire ligand molecules.

Binding ligand prediction for ligand unbound pockets

We have performed an additional experiment for Patch-Surfer on a set of ligand unbound pockets. The purpose of this experiment is to mimic the actual situation in which binding ligand prediction for a protein that does not have bound ligand. We use the Huang dataset (Table IC) because this dataset originates from a list of ligand bound and unbound protein pairs.[34] The RMSD value of ligand bound structure (underlined PDB IDs in the fourth column of Table IC) and ligand-free proteins (the right most column of Table IC) ranges from 0.11 to 0.87 Å with an average value of 0.38 Å. This value is similar to a recent thorough study,[54] which reports the average RMSD of ligand-bound and -unbound form is 0.74 Å. For a query protein structure without bound ligand, a ligand-binding pocket was determined in two ways. In the first method, the ligand-binding pocket taken from the bound structures was superimposed to the unbound structure using the align program in PyMOL (version 1.3). The first method is aimed to examine how the difference of the bound and unbound pocket shape affects to the retrieval accuracy.

Table V
Prediction Success Rates for Ligand Bound and Unbound Pockets of the Huang Dataset

| | Bound proteins[a] | | Unbound proteins | | | |
| | | | Bound ligand position[b] | | LIGSITEcsc prediction[c] | |
Features used	Top1	Top3	Top1	Top3	Top1	Top3
S − − −	0.203 (0.269)	0.588 (0.733)	0.250 (0.333)	0.667 (0.750)	0.417 (0.417)	0.417 (0.500)
S − − − + size	0.190 (0.236)	0.559 (0.606)	0.250 (0.500)	0.667 (0.750)	0.273 (0.273)	0.545 (0.636)
SHEV	0.172 (0.277)	0.555 (0.691)	0.250 (0.417)	0.750 (0.833)	0.250 (0.250)	0.500 (0.500)
SHEV + size	0.169 (0.170)	0.543 (0.592)	0.250 (0.500)	0.750 (0.833)	0.250 (0.322)	0.417 (0.417)

The values shown in parentheses are the prediction success rate computed when FUC, GAL, MAN, and MMA are grouped as SAC (saccharide) (see Fig. 7).
[a]The average values of the results using ligand bound pockets, that is, the data presented in Figure 7, are shown.
[b]Ligand-binding regions were extracted by referring to the corresponding ligand bound pockets.
[c]3appA was not included because LIGSITEcsc did not make a binding site prediction near the MAN binding site.

The second method uses a ligand-binding site prediction method, LIGSITE,[34] to predict the binding site in the unbound protein structure. This is aimed to directly simulate blind prediction when there is no clue in regard to the location of binding sites in the query protein.

Table V summarizes the prediction results. The middle columns show the Top-1 and Top-3 prediction success rate using unbound pockets identified by superimposing ligand bound pockets. Compared with the average success rate of ligand bound pockets previously shown with graphs in Figure 7 (leftmost columns), interestingly, the success rates for the unbound pockets are comparable and in some cases success rates are even better than that of the bound pockets. These findings are consistent with the Pocket-Surfer results shown in our previous work (Fig. 9 of Ref. [29]). As for the results provided by using the predicted ligand-binding pockets (the right most columns), their Top-1 success rate are better, whereas the Top-3 results are worse than the bound pocket results. However, the deterioration of the Top-3 success rate for the predicted pockets is much less than what was observed for Pocket-Surfer (Table 8 in Ref. [29]), where the Top-3 success rate for predicted pockets went down to almost half the success rate of using bound pockets. Thus, the patch representation of pockets is more tolerant to the inaccuracies of predicted binding pockets.

Computation time

The computation time of each step in Patch-Surfer and Pocket-Surfer is summarized in Table VI. The times were evaluated on a desktop computer with an Intel core i7 at 2.67 GHz and 11 GB memory. It takes more time to prepare the pocket model of a query pocket for Patch-Surfer than for Pocket-Surfer because Patch-Surfer represents a query pocket with around 20–40 surface patches, whereas the whole pocket is represented as a single object in Pocket-Surfer. Similarly, the database search by Patch-Surfer against the original Kahraman dataset with 100 pockets took longer than Pocket-Surfer because the former needs identification of similar patches in the query and database pockets using the modified bipartite match-

ing algorithm. We also measured the search speed of a dataset with 200 pockets (by duplicating the original Kahraman dataset), which resulted in 0.046 s and 7.52 s for Pocket-Surfer and Patch-Surfer, respectively. A search speed for a larger pocket database can be computed by extrapolating these two search speeds. For example, a search against 5438 pockets taken from a list of non-redundant ligand-binding protein structures in the Protein-Small-Molecule DataBase[55] (http://compbio.cs.toronto.edu/psmdb/downloads/CPLX_25_0.85_7HA.list) takes 1.04 s and 3 min 23.42 s by Pocket-Surfer and Patch-Surfer, respectively. Thus, although Patch-Surfer takes more time than Pocket-Surfer Patch-Surfer is still practically fast enough for interactive search against a database with a realistic number of entries.

DISCUSSION

In this article, we reported a new binding ligand prediction method, Patch-Surfer, which represents pockets by a group of surface patches to capture local similarity of pockets. Comparison with the previously developed method, Pocket-Surfer, which captures global features of pockets, has highlighted the Patch-Surfer's superior characteristics of identifying pockets of the same ligand type, which do not necessarily have global similarity but similar local surfaces between each other. As shown in Figure 3, ligand-binding pockets contain conserved

Table VI
The Computation Time of Pocket-Surfer and Patch-Surfer

	Process	Pocket-surfer	Patch-surfer
Preparation	Binding site prediction by LIGSITEcsc	3.12 s	3.12 s
	Computation of the descriptor	16 s	1 min 52.96 s[a]
Database	Computing distance to each pocket[b]	0.027 s	3.78 s[a]
	Ligand prediction	0.02 s	0.02 s
Total		31.54 s	2 min 12.26 s

[a]Only shape information is encoded.
[b]Measured on the original Kahraman dataset which contains 100 pockets.

regions as well as diverse regions among different protein structures. Patch-Surfer can identify the conserved regions of the pockets and therefore better detect similarities among pockets that bind to same ligand type. Interestingly, the patch representation is also tolerant to predicted binding pockets, which may not be very precise in location but contain correct local regions of ligand-binding pockets. The use of the 3DZD, a rotational invariant and compact descriptor of 3D object, provided convenient means of representing local surface shape and properties that enabled fast comparison and searches of pockets.

On the other hand, the patch representation occasionally leads to wrong binding ligand predictions, typically by identifying surface patches that bind to the same chemical group in different ligand molecules. Such examples of adenine moiety that is in common to ATP, AMP, FAD, and NAD are shown in Figure 11. Although this is not desirable for binding ligand prediction, the ability of detecting local surface similarities can lead to the development of a novel method that can identify binding sites of chemical groups in protein surfaces. Such a binding chemical group prediction method could be advantageous in predicting the binding of novel ligand molecules that consist of known chemical groups. It will be also very useful in rational drug design.[56] Another direction of future development is to apply the patch-based surface recognition method to the identification of other functional regions in protein surface such as protein–protein-binding and RNA- or DNA-binding regions.

Unlike existing binding ligand prediction methods that mainly rely on global protein structure similarity,[15] Patch-Surfer and Pocket-Surfer identify similarity of local shape and physicochemical properties of binding pockets. Our methods will be effective for annotating structures which do not have global structural and sequence similarity to known proteins. A growing number of protein structures of unknown function in PDB, indeed, do not have apparent global similarity to annotated proteins.

In summary, we have developed a new binding ligand prediction method, Patch-Surfer, which represents a pocket by a set of surface patches described with the 3DZDs. There are three major advantages of Patch-Surfer: first, Patch-Surfer is capable of identifying local similarities in ligand-binding surface regions. This is effective in identifying binding pockets of the same ligand type that are flexible and binds to pockets in different conformations. Second, due to the local pocket surface comparison, the method can predict binding ligands of proteins that do not share apparent global sequence and structure similarity to known proteins in the database. Third, the use of the 3DZD enables fast comparison of binding pockets. We are currently in the process of developing a comprehensive database of binding pockets for more practical use of Patch-Surfer in binding pocket annotation for proteins.[57] Further application of a patch-based approach using the 3DZD will open new perspectives in classification and analysis of biomolecules for biological function annotation.

ACKNOWLEDGMENTS

REFERENCES

1. Hawkins T, Kihara D. Function prediction of uncharacterized proteins. J Bioinform Comput Biol 2007;5:1–30.
2. Hawkins T, Chitale M. New paradigm in protein function prediction for large scale omics analysis. Mol Biosyst 2008;4:223–231.
3. Watson JD, Laskowski RA, Thornton JM. Predicting protein function from sequence and structural data. Curr Opin Struct Biol 2005;15:275–284.
4. Valencia A. Automatic annotation of protein function. Curr Opin Struct Biol 2005;15:267–274.
5. Chikhi R, Sael L, Kihara D. Protein binding ligand prediction using moment-based methods. In: Protein function prediction for omics era. Springer; 2011. pp 145–163.
6. Chitale M, Kihara D. Computational protein function prediction: framework and challenges. In: Protein function prediction for omics era. Springer; 2011. pp 1–17.
7. Chandonia J-M, Brenner SE. The impact of structural genomics: expectations and outcomes. Science 2006;311:347–351.
8. Berman HM, Westbrook J, Feng Z, Gilliland G, Bhat TN, Weissig H, Shindyalov IN, Bourne PE. The protein data bank. Nucleic Acids Res 2000;28:235–242.
9. Wild DL, Saqi MAS. Structural proteomics: inferring function from protein structure. Curr Proteomics 2004;1:59–65.
10. Roberts RJ. Identifying protein function—a call for community action. PLoS Biol 2004;2:e42.
11. Roberts RJ. COMBREX: computational bridge to experiments. Biochem Soc Trans 2011;39:581–583.
12. Gene Ontology Consortium. The gene ontology in 2010: extensions and refinements. Nucleic Acids Res 2010;38:D331–D335.
13. Rosenberg M, Goldblum A. Computational protein design: a novel path to future protein drugs. Curr Pharm Des 2006;12:3973–3997.
14. Samish I, Macdermaid CM. Perez-Aguilar JM, Saven JG. Theoretical and computational protein design. Annu Rev Phys Chem 2010; 62:129–149.
15. Skolnick J, Brylinski M. FINDSITE: a combined evolution/structure-based approach to protein function prediction. Brief Bioinform 2009;10:378–391.
16. Creighton T. Proteins: structures and molecular properties. W.H. Freeman: New York; 1993.
17. Porter CT, Bartlett GJ, Thornton JM. The catalytic site atlas: a resource of catalytic sites and residues identified in enzymes using structural data. Nucleic Acids Res 2004;32:D129–D133.
18. Arakaki AK, Zhang Y, Skolnick J. Large-scale assessment of the utility of low-resolution protein structures for biochemical function assignment. Bioinformatics 2004;20:1087–1096.
19. Ferrè F, Ausiello G, Zanzoni A, Helmer-Citterich M. SURFACE: a database of protein surface regions for functional annotation. Nucleic Acids Res 2004;32:D240–D244.
20. Gold ND, Jackson RM. Fold independent structural comparisons of protein–ligand binding sites for exploring functional relationships. J Mol Biol 2006;355:1112–1124.
21. Shatsky M, Shulman-Peleg A, Nussinov R, Wolfson HJ. The multiple common point set problem and its application to molecule binding pattern detection. J Comput Biol 2006;13:407–428.
22. Hoffmann B, Zaslavskiy M, Vert J-P, Stoven V. A new protein binding pocket similarity measure based on comparison of clouds of

atoms in 3D: application to ligand prediction. BMC Bioinformatics 2010;11:99.

23. Sael L, Kihara D. Protein surface representation and comparison: new approaches in structural proteomics. In: Chen J, Lonardi S. editors. Biological data mining. Chapman & Hall/CRC Press; 2009. pp 89–109.

24. Kinoshita K, Murakami Y, Nakamura H. eF-seek: prediction of the functional sites of proteins by searching for similar electrostatic potential and molecular surface shape. Nucleic Acids Res 2007; 35:W398–W402.

25. Morris RJ, Najmanovich RJ, Kahraman A, Thornton JM. Real spherical harmonic expansion coefficients as 3D shape descriptors for protein binding pocket and ligand comparisons. Bioinformatics 2005;21:2347–2355.

26. Kahraman A, Morris RJ, Laskowski RA, Favia AD, Thornton JM. On the diversity of physicochemical environments experienced by identical ligands in binding pockets of unrelated proteins. Proteins 2010;78:1120–1136.

27. Das S, Kokardekar A, Breneman CM. Rapid comparison of protein binding site surfaces with property encoded shape distributions. J Chem Inf Model 2009;49:2863–2872.

28. Osada R, Funkhouser T, Chazelle B, Dobkin D. Shape distributions. ACM Trans Graphics 2002;21:807–832.

29. Chikhi R, Sael L, Kihara D. Real-time ligand binding pocket database search using local surface descriptors. Proteins 2010;78:2007–2028.

30. Kobayashi N, Go N. A method to search for similar protein local structures at ligand binding sites and its application to adenine recognition. Eur Biophys J 1997;26:135–144.

31. Li B, Turuvekere S, Agrawal M, La D, Ramani K, Kihara D. Characterization of local geometry of protein surfaces with the visibility criterion. Proteins 2008;71:670–683.

32. Canterakis N. 3D Zernike moments and Zernike affine invariants for 3D image analysis and recognition. In: Proceedings of the 11th Scandinavian conference on image analysis, Kangerlussuaq, Greenland; 1999. pp 85–93.

33. Kahraman A, Morris RJ, Laskowski RA, Thornton JM. Shape variation in protein binding pockets and their ligands. J Mol Biol 2007;368:283–301.

34. Huang B, Schroeder M. LIGSITEcsc: predicting ligand binding sites using the Connolly surface and degree of conservation. BMC Struct Biol 2006;6:19.

35. Baker NA, Sept D, Joseph S, Holst MJ, McCammon JA. Electrostatics of nanosystems: application to microtubules and the ribosome. Proc Natl Acad Sci USA 2001;98:10037–10041.

36. Kyte J, Doolittle RF. A simple method for displaying the hydropathic character of a protein. J Mol Biol 1982;157:105–132.

37. Novotni M, Klein R. 3D Zernike descriptors for content based shape retrieval. In: Proceedings of the eighth ACM symposium on solid modeling and applications; 2003. pp 216–225.

38. Venkatraman V, Sael L, Kihara D. Potential for protein surface shape analysis using spherical harmonics and 3D Zernike descriptors. Cell Biochem Biophys 2009;54:23–32.

39. Kihara D, Sael L, Chikhi R, Esquivel-Rodriguez J. Molecular surface representation using 3D Zernike descriptors for protein shape comparison and docking. Curr Protein Pept Sci 2011;12:520–530.

40. Sael L, Li B, La D, Fang Y, Ramani K, Rustamov R, Kihara D. Fast protein tertiary structure retrieval based on global surface shape similarity. Proteins 2008;72:1259–1273.

41. La D, Esquivel-Rodriguez J, Venkatraman V, Li B, Sael L, Ueng S, Ahrendt S, Kihara D. 3D-SURFER: software for high-throughput protein surface comparison and analysis. Bioinformatics 2009; 25:2843–2844.

42. Sael L, La D, Li B, Rustamov R, Kihara D. Rapid comparison of properties on protein surface. Proteins 2008;73:1–10.

43. Venkatraman V, Chakravarthy PR. Application of 3D Zernike descriptors to shape-based ligand similarity searching. J Cheminform 2009;1:1–19.

44. Venkatraman V, Yang YD, Sael L, Kihara D. Protein–protein docking using region-based 3D Zernike descriptors. BMC Bioinform 2009;10:407.

45. Sael L, Kihara D. Protein surface representation for application to comparing low-resolution protein structure data. BMC Bioinform 2010;11:S2.

46. Yin S, Dokholyan NV. Fingerprint-based structure retrieval using electron density. Proteins 2010;79:1002–1009.

47. Sael L, Kihara D. Characterization and classification of local protein surfaces using self-organizing map. Int J Knowl Discov Bioinformatics 2010;1:32–47.

48. Sael L, Kihara D. Binding ligand prediction for proteins using partial matching of local surface patches. Int J Mol Sci 2010;11:5009–5026.

49. Demange G, Gale D, Sotomayor M. Multi-item auctions. J Polit Econ 1986;94:863–872.

50. Gold ND, Jackson RM. Fold independent structural comparisons of protein–ligand binding sites for exploring functional relationships. J Mol Biol 2006;355:1112–1124.

51. Minai R, Matsuo Y, Onuki H, Hirota H. Method for comparing the structures of protein ligand-binding sites and application for predicting protein–drug interactions. Proteins 2008;72:367–381.

52. Xiong B, Wu J, Burk D, Xue M, Jiang H, Shen J. BSSF: a fingerprint based ultrafast binding site similarity search and function analysis server. BMC Bioinformatics 2010;11:47.

53. Shindyalov IN, Bourne PE. Protein structure alignment by incremental combinatorial extension (CE) of the optimal path. Protein Eng 1998;11:739–747.

54. Brylinski M, Skolnick J. What is the relationship between the global structures of apo and holo proteins? Proteins 2007;70:363–377.

55. Wallach I, Lilien R. The protein-small-molecule database, a non-redundant structural resource for the analysis of protein–ligand binding. Bioinformatics 2009;25:615–620.

56. Li YY, Hou TJ, Goddard WA, III. Computational modeling of structure–function of G protein-coupled receptors with applications for drug design. Curr Med Chem 2010;17:1167–1180.

57. Sael L, Kihara D. Constructing patch-based ligand-binding pocket database for predicting function of proteins. BMC Bioinformatics 2012, in press.